RESEARCH ARTICLE | NOVEMBER 23 2020

Al Kα XPS reference spectra of polyethylene for all instrument geometries

Special Collection: Special Topic Collection: Reproducibility Challenges and Solutions

Alexander G. Shard ; Benjamen P. Reed

Journal of Vacuum Science & Technology A 38, 063209 (2020)
https://doi.org/10.1116/6.0000578

JVST A
Journal of Vacuum Science & Technology A

ARTICLE

avs.scitation.org/journal/jva

Al Kα XPS reference spectra of polyethylene for all instrument geometries

Cite as: J. Vac. Sci. Technol. A 38, 063209 (2020); doi: 10.1116/6.0000578
Submitted: 24 August 2020 · Accepted: 30 October 2020 ·
Published Online: 23 November 2020

Alexander G. Shard[a] and Benjamen P. Reed

AFFILIATIONS

National Physical Laboratory, Hampton Road, Teddington TW11 0LW, United Kingdom

Note: This paper is part of the Special Topic Collection on Reproducibility Challenges and Solutions.
[a]**Author to whom correspondence should be addressed:** alex.shard@npl.co.uk. **Tel.:** +44 (0)20 8943 6193

ABSTRACT

This paper extends a previous description of XPS survey spectra from low density polyethylene (LDPE), which was specific for a single type of geometry, to all geometries. Instrument geometries are specified by two angles. The first angle, a, is between the sample-to-monochromator vector and the sample-to-analyzer vector. The second angle, b, is the dihedral angle between the anode-monochromator-sample plane and the monochromator-sample-analyzer plane. The second angle is important because of the polarization induced by the monochromator. We show, using theory, that the XPS spectrum can be decomposed into a "magic angle" reference spectrum, I_1, and an anisotropy correction spectrum, f. The geometry for LDPE at which photoemission intensity is equivalent to isotropic emission is shown to be a function of a and b with extreme values for a of 64.6° ($b = 0$ or 180°) and 57.5° ($b = 90°$). The deviation of these angles from the "magic angle" $a = 54.7°$ is due to a combination of x-ray polarization and nondipole effects in photoemission. Intensity-calibrated data from a number of instruments with two geometries with $b = 180°$, one set with $a = 60°$ and the other set with $a = 45°$ are used to determine I_1 and f, and these are fitted with simple functions to allow the reproduction of LDPE reference spectra for any instrument geometry. The spectra are taken from the Versailles Project on Advanced Materials and Standards, Technical Working Area 2: Surface Chemical Analysis study A27 and are traceable to the National Physical Laboratory, UK intensity calibration spectra for argon ion sputter-cleaned gold. The functions in this paper may be used in the calibration of XPS instruments with quartz-crystal-monochromated Al Kα x-rays by the comparison of the calculated reference spectrum to data from clean LDPE.

I. INTRODUCTION

The most common form of surface chemical analysis is XPS.[1] It is routinely used as a characterization method for a wide range of engineering and sciences, where the properties of surfaces, thin films, and interfaces are important. It is of increasing importance that the data from an XPS instrument can be converted into a meaningful measurement, and this requires an intensity calibration method for the instrument which accounts for the instrumental geometry. This calibration is essential whenever XPS data are to be directly compared to results taken using different settings of the same instrument, using a different instrument or using theoretical calculations. The use of relative sensitivity factors from literature sources is an example of such a comparison and, without a common calibration scheme for the two instruments, errors can exceed a factor of 2.

The most practical method to calibrate the intensity scale of an instrument is to perform a survey scan across the useful kinetic energy range of the instrument using a clean reference sample. The measured intensity at selected energies can then be compared to a reference intensity and the energy-dependent response of the instrument, which is commonly termed the "transmission function" can be established.[2] The transmission function is defined in ISO 18115-1 as "quotient of the number of particles transmitted by the analyser by the number of such particles per solid angle and per interval of the dispersing parameter (in this case, energy) available for measurement as a function of the dispersing parameter." The correct term is a "spectrometer response function," which also accounts for detector efficiency. For an XPS instrument operating in a constant analyzer energy (fixed analyzer transmission) mode, the detection efficiency is assumed to be constant. The most commonly used reference materials for this purpose are copper, silver, and gold.[3,4] Using such methods, the repeatability and reliability of data from an instrument can be

ensured.[5] While this seems straightforward, there are several issues that need consideration.

(1) There are no commonly available reference spectra. Different instrument manufacturers use their own calibration schemes which are, often, not comparable to other calibration methods.
(2) Reference spectra are dependent upon the geometry of the XPS instrument due to the variation in angular distributions of emitted photoelectrons. Therefore, a unique reference spectrum is required for each reference material and instrument geometry. These were built into the NPL (National Physical Laboratory, UK) calibration software[6] that was available until the software became incompatible with modern operating systems. The software had several users but the reference spectra, which included additional spectra for the effects of the polarization of the monochromated x-ray beam, were not separately available.

In addition to these issues, many practical details need to be attended to. These are detailed in the main paper describing the Versailles Project on Advanced Materials and Standards, Technical Working Area 2 (VAMAS TWA2): Surface Chemical Analysis A27 study[7] and include dark noise, scattering in the spectrometer,[8] sample cleaning protocols, and detector saturation. The latter two are particular problems for noble metal reference materials because not all spectrometers are equipped with sputter ion sources and the efficiency of modern spectrometers, combined with the yield of photoelectrons from noble metals is sufficient to saturate detectors even in the background, away from the peaks in the spectrum. Recently, we published a reference spectrum described by a mathematical function of electron kinetic energy for clean low density polyethylene (LDPE), which was suitable for calibrating instruments of a particular geometry.[9] That geometry was with a 60° monochromator-sample-analyzer angle and with the anode, monochromator, sample, and analyzer all in the same plane. In this paper, we term that geometry $[a,\ b] = [60°,\ 180°]$, as explained later. One of the aims of the VAMAS TWA2 A27 study was to establish whether LDPE could be used as a reference material for other instruments and, for this purpose, it is necessary to investigate the effects of instrument geometry on the LDPE spectrum and find a way to describe them mathematically.

The specific advantages of LDPE over noble metals as a reference material are that it is easy to clean *ex situ* (it does not require a sputter source on the instrument), it is relatively free from photoelectron peaks (which should not be used in calibration and produce "gaps" in the calibration), and it is insensitive to adventitious hydrocarbon contamination (partly due to surface energy, partly because it is a pure hydrocarbon). It produces a low intensity spectrum, which enables calibration at the normal operating power of the anode; however, this also introduces statistical uncertainty and sensitivity to dark noise contributions, particularly in the very low intensity region above ~1200 eV kinetic energy. The fact that LDPE consists of light elements and has low elastic scattering makes the calculations presented below more accurate.

II. THEORY

The angular distribution of photoelectrons which are emitted without energy loss from a given subshell of uniformly distributed atoms in a homogeneous solid using plane-polarized x-rays with the electric field vector in direction "A" may be represented by the relationship given in (1),

$$I_A \propto J_A \lambda_E \sigma S[1 + sF_A], \tag{1}$$

in which I_A is the photoelectron intensity for the peak, J_A is the x-ray flux, λ_E is the energy-dependent inelastic mean free path of the electrons in the solid, σ is the photoionization cross section for the relevant subshell. S and s are correction factors[10–12] which account for the effects of elastic scattering on the intensity and angular distribution of electrons. These factors depend upon the single-scattering albedo, ω and upon the electron emission angle. The emission-angle dependence is rather weak, for polyethylene less than 2% change in S and s, except for emission angles larger than ~60° (take-off angles lower than ~30°). The anisotropic distribution of photoelectrons[13] is captured by the term F_A, which is given in Eq. (2), in which β is the dipole asymmetry parameter and γ and δ account for nondipole emission. θ_A is the angle between the photoelectron vector and ϵ_A, the electric field vector of the x-rays. ϕ_A is the angle between the photon momentum vector and the projection of the photoelectron vector onto the plane normal to ϵ_A. These angles are depicted in Fig. 1(a) and a similar figure can be constructed to illustrate θ_B and ϕ_B in relation to the vector ϵ_B, which is orthogonal to ϵ_A,

$$F_A = \frac{\beta}{2}(3\cos^2\theta_A - 1) + (\delta + \gamma\cos^2\theta_A)\sin\theta_A\cos\phi_A. \tag{2}$$

For partially polarized x-rays, we may write an analogous equation for electron emission for x-rays with an electric vector ϵ_B orthogonal to ϵ_A and obtain the summed total emission, $I = I_A + I_B$ in a given direction, which is expressed in (3) using the sum $J = J_A + J_B$ and the degree of polarization in direction ϵ_A is expressed as $P_A = J_A/J$,

$$I \propto J\lambda_E\sigma S[1 + s(P_A F_A + \{1 - P_A\}F_B)] = J\lambda_E\sigma S[1 + sG]. \tag{3}$$

It is more convenient to express the function G in terms of angles which are used to describe instrument geometries. These are shown in Figs. 1(b) and 1(c). Here, we term the monochromator-sample-analyzer angle as a (more commonly this is termed β, but here we use that symbol for a photoionization parameter) and the dihedral angle between the monochromator-sample-analyzer plane and the anode-monochromator-sample plane as b (more commonly this is ξ). After some simplification, which is detailed in the Appendix, we arrive at Eq. (4). If the nondipole terms γ and δ are set to zero, this is mathematically identical to a previous description of the effect of monochromator polarization on photoemission,[14]

$$G = -\frac{\beta}{2} - \delta\cos a + \left(\frac{3\beta}{2} - \gamma\cos a\right) \times \left[\frac{1}{2} + \left(P_A - \frac{1}{2}\right)\cos 2b\right]\sin^2 a. \tag{4}$$

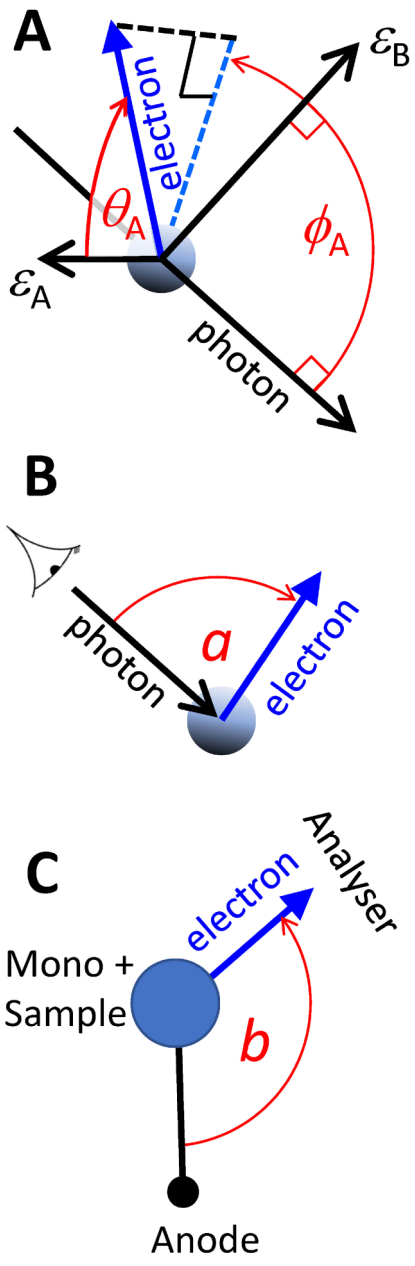

FIG. 1. Pictorial depiction of the angles used in this paper. (a) Three-dimensional figure with orthogonal axes "photon," ϵ_A and ϵ_B. The vector ϵ_A is directed toward the reader. The photoemission vector is represented by the solid arrow labeled "electron" which is also out of the plane of the paper: θ_A is the angle between the outgoing electron and the electric vector; φ_A is the azimuthal angle in the plane normal to the electric vector. (b) Instrument geometry with all lines in the plane of the paper, a is the angle between the incoming photon and outgoing electron into the analyzer. The monochromator is in the direction of the pictorial eye. (c) Schematic from the point of view of the eye in (b), along the photon vector from the monochromator and with the anode pointing down. b is the dihedral angle between the anode-monochromator-sample plane and the monochromator-sample-analyzer plane.

The value of P_A can be found using Eq. (5) using the assumption that the quartz crystal is a perfect Bragg reflector and setting $b = 0$ as in Fig. 1(c) such that $J_A < J_B$,

$$P_A = \frac{\cos^2\left[2\arcsin\left(\frac{\lambda_{ph}}{2d}\right)\right]}{1+\cos^2\left[2\arcsin\left(\frac{\lambda_{ph}}{2d}\right)\right]}, \tag{5}$$

in which d is the spacing of the crystal plane and λ_{ph} is the wavelength of the x-ray. For Al Kα x-rays ($\lambda_{ph} = 8.340$ Å) and a quartz (10−10) crystal ($2d = 8.514$ Å), $P_A = 0.458$. We also consider the potential effects of the finite angular range of x-rays impinging on the sample and the angular range of electron collection into the analyzer. This is described in the Appendix and could contribute to an error of the order of 1% for very large (30°) collection angles but is not large enough to explicitly include in this analysis.

In terms of simplicity, it is fortunate that the angular asymmetry parameters of C 1s and C 2s are very similar. Literature values[13] for a photon energy of 1500 eV may be used with negligible error. The mean values for β, γ, and δ are, respectively, 1.99 ± 0.01, 0.765 ± 0.01, and approximately zero. The contribution of intensity from other orbitals is small, for example, C 2s is approximately an order of magnitude more intense than C 2p and, therefore, common values for β, γ, and δ can be used. This does not apply to Auger emission, in which case the emission is isotropic and this can be dealt with by setting s to zero. Putting the explicit values into Eq. (4), we obtain Eq. (6),

$$G(\text{carbon}) = (2.99 - 0.765\cos a)[0.5 - 0.042\cos 2b]\sin^2 a - 0.995\,. \tag{6}$$

This function is plotted in Fig. 2 with the two extreme values of $b = 0$ or 180° and $b = 90°$ as solid and dashed lines, respectively. In the figure, two of the most common geometries encountered during the VAMAS study, $a = 45°$ and $a = 60°$, both with $b = 180°$, are marked by vertical dotted lines and circles with values of $G = -0.434$ and $G = -0.099$, respectively. There are two positions in each curve where $G = 0$: with $b = 0$ or 180° these are $a = 64.6°$ and 127.5°, with $b = 90°$ these are $a = 57.5°$ and 133.8°. These represent the essential "magic angles" for the XPS of LDPE using Al Kα x-rays and a quartz crystal monochromator. Both x-ray polarization and nondipole terms in photoemission cause a deviation from the expected $a = 54.7°$ "magic angle." A spectrum taken in these geometries would be expected to have $G = 0$ and the photoionization peak intensities proportional to the product $J\,\lambda_E\,\sigma\,S$. We designate this "geometry-free" spectrum I_1 and assume that the full spectrum can be obtained from Eq. (7) using values of G calculated from Eq. (6),

$$I = I_1[1 + fG]. \tag{7}$$

This expression has been developed for photoelectron emission without energy loss, with the corrections S and s for elastic scattering incorporated into the expression. The energy dependent function f replaces the term s in the expression to account for angular anisotropy and is expected to be equivalent to s only for

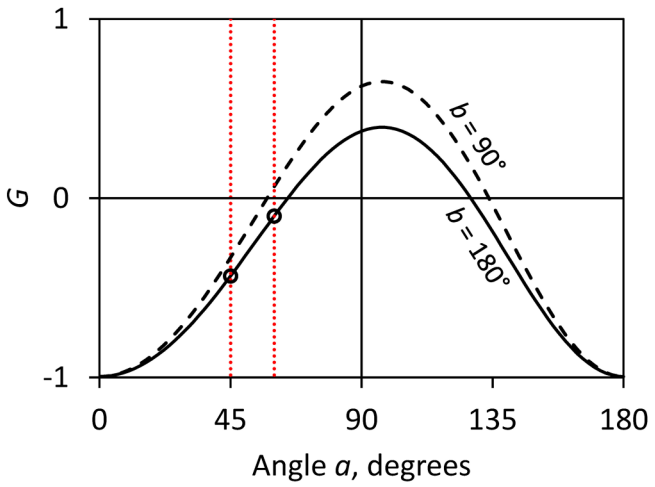

FIG. 2. Graph of Eq. (6), G, for C 1s and C 2s. The normal geometry, $b = 0$ or 180° is plotted as a solid line and the other extreme geometry for $b = 90°$ as a dashed line. All instruments fall between these two lines. The common geometries of $a = 45°$ and $a = 60°$, both with $b = 180°$ are marked with dotted vertical lines and circles.

photoelectron peaks on a negligible inelastic background. This replacement may be considered valid for the inelastic background because the anisotropy of the original emission is retained but gets weaker as the path length in the solid increases. From these simple considerations, we would expect that the value of f for the background will be similar to that of the photoelectron peak close to the peak but decline toward zero at kinetic energies lower than the peak. Intuitively, it is difficult to see how the value of f could be negative but since this is observed in the data the possibility requires explanation.

For electrons in the background, we should be concerned with two general classes of electrons: those that are originally emitted in the direction of the analyzer and those that are scattered into the direction of the analyzer and then leave the surface. If there were no elastic scattering, then only the first class of electrons will reach the detector. If, also, the mean energy loss per inelastic collision is constant with electron energy, the background intensity will be proportional to the inelastic mean free path at the kinetic energy of the emitted electron. It would also be proportional to the photoelectron peak intensity (f would be 1 for the peak and the background). Lower-kinetic-energy electrons in the inelastic background would, on average, come from deeper in the sample than higher-kinetic-energy electrons because higher-kinetic-energy electrons generate the lower-kinetic-energy electrons after some additional distance traveled through the sample. With elastic scattering, the intensity of such "straight line" electrons will decrease due to directional change, which will be more significant for electrons which travel further. Deep within the material, these scattered electrons will be replaced by other electrons scattered into the direction of the analyzer. The two processes, which by symmetry occur with equal probability, will equalize populations traveling at different angles and tend toward an equilibrium isotropic distribution with $f = 0$. However, near the surface, progress toward equilibrium may be less straightforward. This is because there is an additional anisotropy caused by downward traveling electrons not being replaced by emission from regions above the surface.

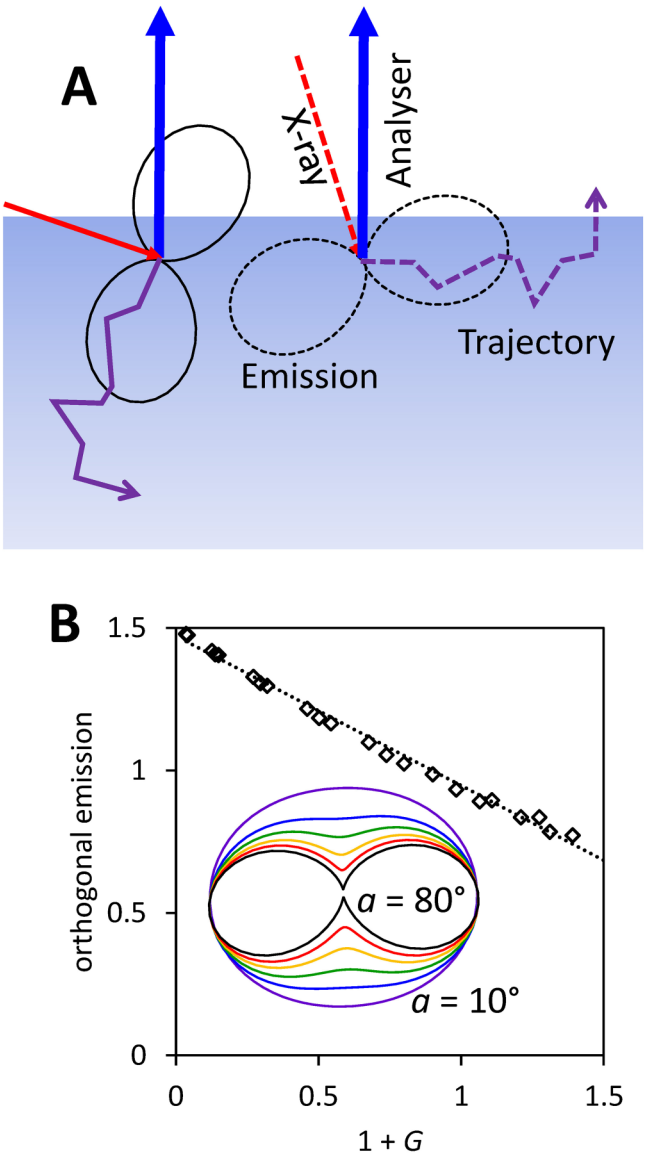

FIG. 3. (a) Schematic of C 1s photoemission in the monochromator-sample-analyzer plane. The incoming arrows depict x-rays impinging on the sample at different angles and the distorted hourglass shapes depict the angular distribution of photoelectron emission in this plane. The jagged arrows show an example electron trajectory in the direction of high emission intensity. (b) Plot of mean emission intensity orthogonal to the analyzer direction against emission intensity directly toward the analyzer ($1 + G$) for a variety of a and b angles. The dotted line is a linear fit. The inset depicts the angular distributions for $b = 0$ and a = 10°, 30°, 40°, 50°, 60°, and 80°.

Figure 3(a) depicts photoemission from C 1s with two incident angles of x-rays and the sample normal to the analyzer. The angular emission distribution is shown in both cases. In this plane, the larger angle of a (solid lines) generates significant intensity in the detected peak, as well as undetected "downward" intensity into the sample. After scattering and energy loss, very few of these downward traveling electrons will reach the detector. With a small angle of a (dashed lines), most of the electrons are traveling parallel to the surface and, after scattering and energy loss, have a larger probability of being emitted into the analyzer. Therefore, we should concern ourselves with the population of electrons that travel sideways in the sample. We require the set of angles a' and b' that are orthogonal to the analyzer. These may be calculated from the equations in the appendix and the two-dimensional angular distributions, $1 + G'$, are plotted as an inset to Fig. 3(b). Figure 3(b) plots the mean emission intensity in the directions orthogonal to the analyzer against the straight line emission intensity $(1 + G)$. The result is an excellent linear correlation with slope -0.525 and $R^2 = 0.993$. It is possible that the sideways electrons start to be important for electron emission into the analyzer, especially at low electron kinetic energies, when the single-scattering albedo rises by a factor of ~5 from its value at the C 1s peak. However, because of the linear correlation shown in Fig. 3(b), this can be compensated using a reduced, or even negative, value of f.

Thus, the inelastic background of LDPE for any instrument geometry can be constructed from two energy-dependent expressions I_1 and f. For pure carbon materials like diamond and graphite, Jablonski[10] suggests that ω is ~0.06, and this provides an expected value of $f \approx s = 0.93$ for the peaks. However, LDPE is significantly less dense than these materials and contains a large proportion of hydrogen therefore ω should be smaller and consequently f should be closer to 1. At kinetic energies lower than the photoelectron peak, the value of f should decline as explained above. Because the C KLL emission is isotropic, this can also be accommodated entirely within I_1, but we may expect a change in f in that region as the angular distribution of electrons close to the surface could alter at, and below, the C KLL kinetic energy.

To extract the energy-dependent values of I_1 and f, we require two calibrated spectra, I_M and I_N, taken at two known and different geometries with geometry factors G_M and G_N. Calibrated spectra need to be acquired on an instrument with a known transmission function and corrected for that transmission. At each kinetic energy I_1 and f maybe found by writing Eq. (7) and solving the resulting simultaneous equations, the solutions are given in Eqs. (8) and (9), in which I_1' and f' are the experimentally derived analogues of I_1 and f,

$$I_1' = \frac{G_N I_M - G_M I_N}{G_N - G_M}, \tag{8}$$

$$f' = \frac{I_M - I_N}{(G_M - G_N) I'_1}. \tag{9}$$

III. REFERENCE SPECTRA

The VAMAS interlaboratory A27 study provided a large number of datasets of both clean gold and clean LDPE using the

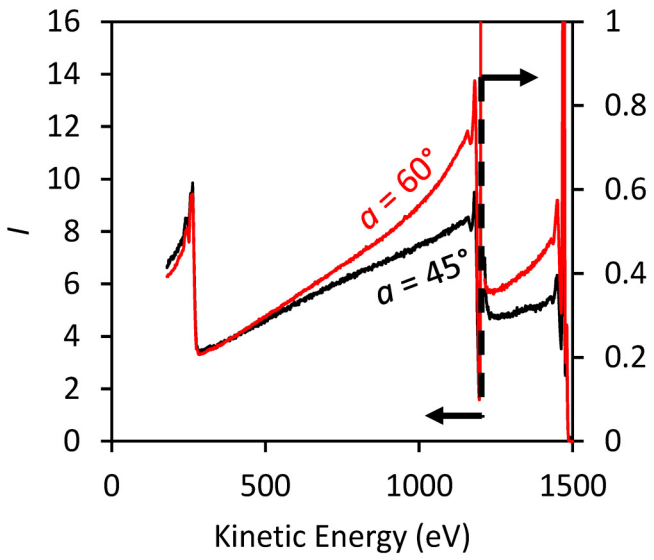

FIG. 4. Two VAMAS LDPE reference spectra. The [60°, 180°] spectrum has higher intensity above 500 eV kinetic energy and the [45°, 180°] spectrum is the lower curve in the same range. The intensity scale is on the left hand side for kinetic energies less than 1201 eV and on the right hand side for higher kinetic energies.

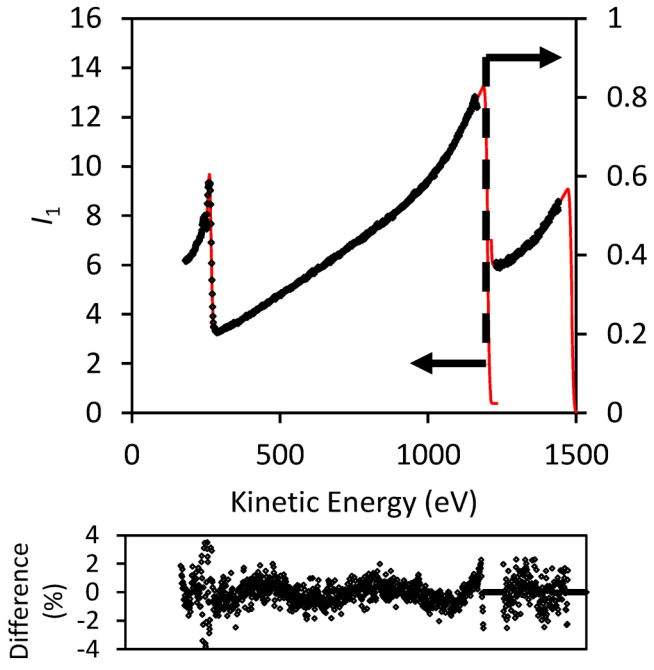

FIG. 5. Extrapolated $G = 0$ spectrum, I_1', as data points and a smooth description, I_1, Eq. (10), shown as a line, the relative difference between the data and the description is shown below the graph.

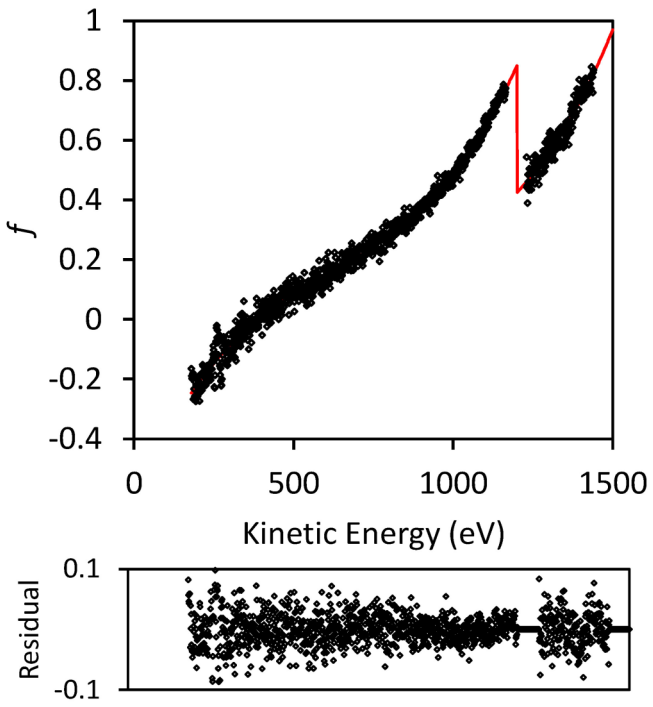

FIG. 6. Calculated geometry correction, f', as data points and a smooth description, f, Eq. (11), shown as a line, the residual between the data and the description is shown below the graph.

same instrument and operating conditions. The most common geometries used by participants in the study were $[a, b] = [60°, 180°]$ and $[a, b] = [45°, 180°]$ for which $G = -0.099$ and $G = -0.434$, respectively, as described above. Spectra were selected from the participants using the following criteria: the gold spectrum showed no evidence of contamination; the LDPE showed no evidence of contamination and division of the gold spectrum by the relevant NPL reference spectrum[6] provided a smooth transmission function fit with little deviation in the ratio of spectra from that fit. The LDPE spectrum was divided by the transmission function fit to provide a calibrated LDPE spectrum with an associated error of less than 5%. The mean spectra for each geometry were obtained from these selected spectra and the relative standard errors of the mean data points within the two mean spectra were less than 3% across the [45°, 180°] spectrum and less than 2% across the [60°, 180°] spectrum. This metric is somewhat influenced by noise in some of the spectra and, therefore, is an overestimate of the error, provided that there is no systematic bias in this procedure. The two spectra, with a change in intensity scale at the C 1s peak, are plotted in Fig. 4 with the intensities in units of I_X, consistent with the NPL calibration method.

We use Eqs. (8) and (9), setting $M = [60°, 180°]$ and $N = [45°, 180°]$ to find: $I_1' = 1.296I_M - 0.296I_N$ and $f' = 2.985\ (I_M - I_N)/I_1$. The results for the background and Auger electron regions are shown in Figs. 5 and 6 as black data points. In Figs. 4–6 the peaks are not emphasized because it is the background that is essential for instrument calibration. Nevertheless, the peak areas are important comparators to the theory used in this paper and the C 1s and C 2s peak areas are provided in Table I along with the derived values of I_1' and f'. The value of I_1' may be in significant error due to the background subtraction method and the neglect of shake up structure; however, the precision of the measurements are important for obtaining the values of f' and these are indicated in the table. The values of f' are found to be within the expected range of $f' > 0.93$, i.e., greater than elemental carbon and $f' < 1$, i.e., less than carbon gas. This result provides some confidence in the consistency of the spectra. Additionally, the intensity of the C KLL Auger electron peaks is identical in the two spectra I_A and I_B, as expected. This situation is most easily visualized in Fig. 6, which is simply a scaled difference spectrum and in which the position of the Auger electron peak is hardly discernible.

TABLE I. Peak areas of the C 1s and valence band (C 2s) using linear background subtraction with uncertainties to indicate the standard error of the mean. Calculated values of I_1' and f' are derived using Eqs. (8) and (9).

Peak	I_A (I_X.eV), 60°	I_B (I_X.eV), 45°	I_1' (I_X.eV)	f'
C 1s	224 ± 4	145 ± 2	247 ± 4	0.95 ± 0.05
Valence band	7.38 ± 0.20	4.76 ± 0.08	8.15 ± 0.21	0.96 ± 0.07

The values for f' within the background, shown in Fig. 6, are smaller than that for the peaks and are well described by an exponential decay, as will be shown in the next section. It is notable that f' reaches zero at the energy of the KLL Auger electron peak and therefore no sharp changes in f' are evident at that point. This is fortuitous from a perspective of describing the curve with a smooth function. Below the Auger electron peak, the value of f' becomes negative and this possibility was discussed previously in association with Fig. 3. Due to the variability in absolute intensity between the sets of data (~5%), we investigated the possibility that this negative f' was due to an intensity scaling error between the [60°, 180°] spectrum and the [45°, 180°] spectrum. This appears to be implausible, first because the intensity change required to make f' positive across the full range is ~10% and even a small intensity change of 3%, in line with the typical

TABLE II. Parameters for Eq. (10) to describe I_1.

I	1	2	3
Values for step functions			
Feature	C KLL	C 1s	Valence
Intensity, d_i	$1.47I_X$	$0.665I_X$	$0.0143I_X$
Decay energy, e_i	228 eV	420 eV	400 eV
Constant, g_i	0	2.51	0
Position, h_i	264 eV	1201 eV	1485 eV
Values for the normal distributions representing peaks			
Peak	C KLL (minor)	C KLL (major)	Broad peak
Area, k_i	7.33 I_X eV	45.5 I_X eV	684 I_X eV
Position, l_i	242.6 eV	263.8 eV	678 eV
Sigma width, m_i	4.6 eV	4.9 eV	229 eV

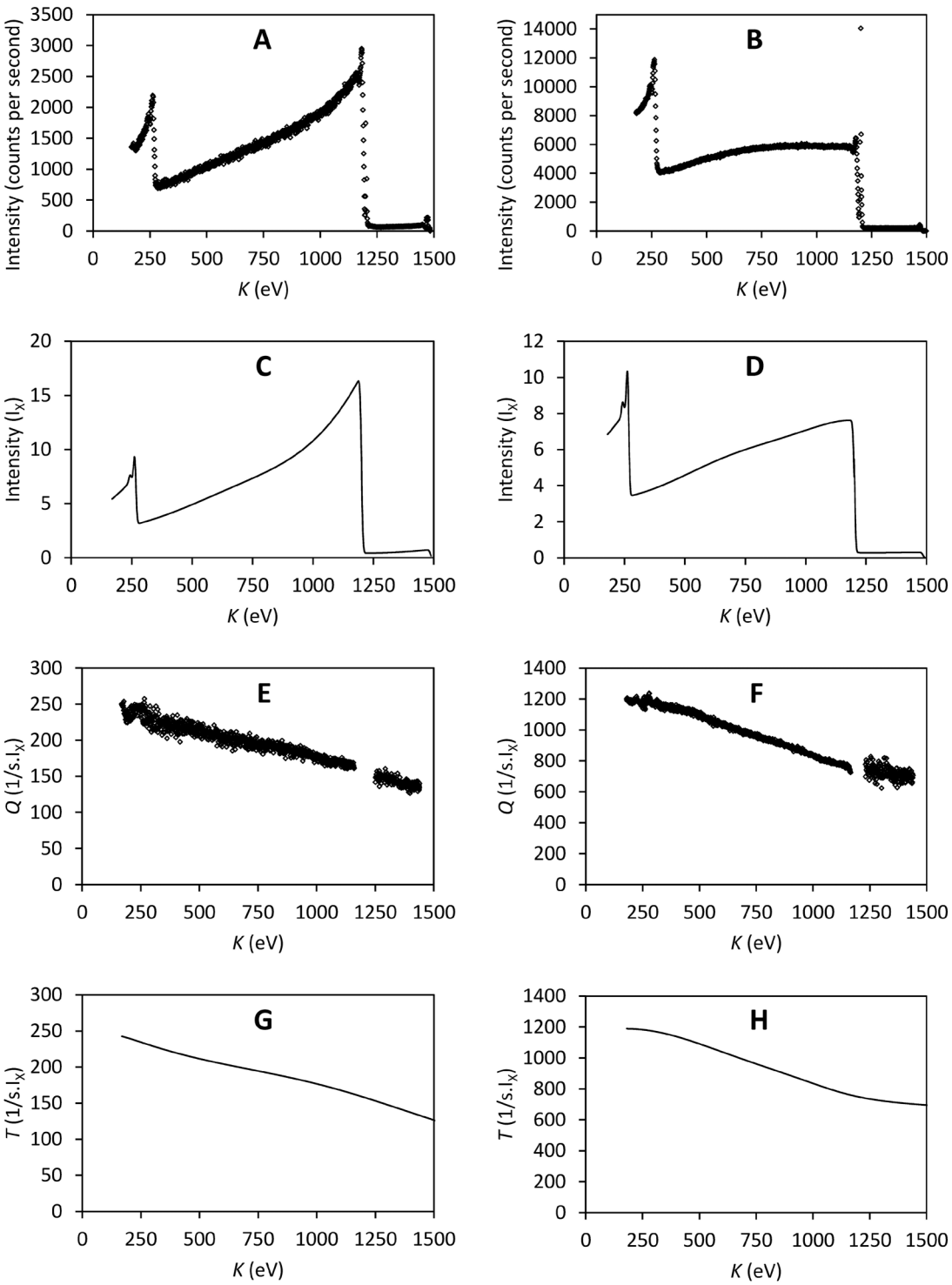

FIG. 7. (a, b) LDPE spectra from two VAMAS participants using instruments with [a, b, G] = [70.8°, 118°, 0.283] and [41°, 180°, −0.519] respectively. (c, d) Reference spectra generated using Eq. (7) and G = 0.283 and −0.519, respectively. (e, f) Q for the two instruments calculated using the ratio of the data to reference spectra in (a, c) and (b, d) respectively. (g, h) T, a rational function which is fitted to Q from (e) and (f) respectively.

standard error of the mean in the data, results in f' having an unphysical value for the C 1s peak.

IV. NOISE-FREE DESCRIPTION OF REFERENCE SPECTRA

The extracted data for I_1' and f' were fitted with functional forms, using the Solver add-in in Excel to optimize parameters. The data were truncated to avoid the highly structured regions around the peaks, specifically the region between 1165 and 1230 eV kinetic energy (256.6–321.6 eV binding energy) and data with kinetic energies above 1440 eV (below 46.6 eV binding energy) were excluded from fits. The fits provide smooth mathematical descriptions I_1 and f across the full energy range, excluding the C 1s and valence band regions. The description for I_1 was based on the same functional form as that used previously for the [60°, 180°] geometry,[9]

$$I_1 = \sum_{i=1}^{3}\left(\left\{d_i\left[\exp\left(\frac{K}{e_i}\right)+g_i\right]\left[1-\Phi\left(\frac{K-h_i}{5}\right)\right]\right\}+\left\{k_i\varphi\left(\frac{K-l_i}{m_i}\right)\right\}\right), \tag{10}$$

in which $K = E + q$, where E is the kinetic energy of electrons from an uncharged surface and q is the static charge on the PE which alters the observed kinetic energies of the electrons. The terms d_i to m_i are constants which are required to reproduce the geometry-free reference PE spectrum. The capital phi, Φ, indicates a cumulative normal distribution. In Eq. (10) it has mean h_i and a standard deviation of 5 eV. The lower case phi, φ, indicates a normal distribution (normalized Gaussian) with mean l_i and standard deviation m_i. Through minimization of the root mean square (RMS) of the relative difference between the curve and the data, parameters for Eq. (10) were found that provided an RMS relative difference less than 0.9%. These are listed in Table II and the curve is shown as the red line in Fig. 5, the relative difference between the curve and the data is shown below the graph. This demonstrates some small systematic differences, which typically remain below the 1% level.

The functional form for f is simpler, consisting of exponential functions rising to the C 1s and valence band peaks and discontinuous at the C 1s peak. A smooth description of the low kinetic energy change to negative f is included. The values in these equations were found by minimizing the RMS absolute difference between the description and the data, fixing the 1201 eV energy for the C 1s, and constraining the characteristic energies in the exponential functions to be identical. Equation (11) is shown as a red line in Fig. 6 and the absolute difference shown as the residual below the graph. The residual shows no systematic structure and is dominated by experimental noise,

$$\varepsilon < 1201\,\text{eV}: f = 0.852\exp\left(\frac{K-1201}{363}\right) - 1.18\left[1-\Phi\left(\frac{K}{270}\right)\right],$$
$$\varepsilon > 1201\,\text{eV}: f = 0.852\exp\left(\frac{K-1453}{363}\right). \tag{11}$$

V. APPLICATION OF REFERENCE SPECTRA

The LDPE reference spectrum for any XPS geometry can be calculated through finding the angles a and b for the instrument and calculating G through Eq. (6). Then Eqs. (10), (11), and (7) may be used to find the reference spectrum, I, in the kinetic energy ranges of 180–1165 eV and 1230–1440 eV. Experimental data from clean LDPE should then be acquired from the instrument, paying attention and care to surface cleanliness, dark noise, scattering in the spectrometer and noise in the data. The latter is particularly important in the high kinetic energy region. The experimental data should be divided by the calculated spectrum to provide a representation of the transmission function. This can then be fitted with a smooth function which may be used to correct other data taken on the same instrument. These steps are described both in the earlier paper for [60°, 180°] instruments[8] and in the report on the VAMAS study which implements the method described in this paper. Figure 7 pictorially illustrates these steps for two instruments in the study with geometries [41°, 180°] and [70.8°, 118°] and associated values of G of −0.519 and 0.283, respectively, demonstrating that sensible results are obtained outside the range of the reference geometries indicated in Fig. 2. The comparability of these transmission functions to those obtained using gold as a reference material is good and a full assessment of comparability across a wider range of geometries is provided in the main paper describing the VAMAS TWA2 A27 study along with the technical details of how to apply the calculated reference spectra.[7]

VI. CONCLUSIONS

In this paper, we have demonstrated that it is possible to describe the majority of a calibrated XPS spectrum of low-density polyethylene from any instrument using only two energy-dependent functions, I_1 and f. These are provided in Eqs. (10) and (11), respectively. One of the functions, I_1, describes the intensity for a "magic angle" geometry and the second, f, describes a correction to account for angular anisotropy in the emitted intensity. The instrument geometry is encapsulated in a value, G, which can be calculated from the known instrument configuration using Eq. (6). Equation (7) combines G, I_1, and f to give a noise free reference spectrum of LDPE, I, suitable for the instrument. The reference spectrum does not include discrete structure near the photoemission peaks for the C 1s, near 1201 eV, and the valence band region. The functional form for the polyethylene XPS spectrum may be used to calibrate XPS instruments using a spectrum taken from a clean LDPE sample on that instrument with the sample directly facing the analyzer.

ACKNOWLEDGEMENTS

This work was funded by the "Metrology for Advanced Coatings and Formulated Products" theme No. NMS/ST20 of the National Measurement System of the UK Department of Business, Energy and Industrial Strategy (BEIS). We gratefully acknowledge Martin Seah, NPL and Steve Spencer, NPL for helpful discussions and advice. We thank participants in the VAMAS study for providing the data essential to this paper: Sven Schroeder, Elizabeth Willneff, and Andrew Britton, *University of Leeds*, UK; Li Yang,

Xi'an Jiaotong Liverpool University, China; Jian Chen and Fangyen Xie, *Sun Yat-sen University*, China; Yusuke Yoshikawa, *Yazaki Corporation*, Japan; Matthew Linford and Tahereh Avval, *Brigham Young University*, USA; Giacomo Ceccone and Francesco-Sirio Fumagalli, *Joint Research Centre*, Ispra, EU; Graham Smith, *University of Chester*, UK; Marc Walker, *University of Warwick*, UK; Bill Theilacker, *Medtronic*, USA; Alberto Herrera Gómez, *CINVESTAV Unidad Querétaro*, Mexico; Dave Castner, *University of Washington*, USA; Emily Smith, *University of Nottingham*, UK; Gilad Zorn, *GE Research*, USA; Ji Sheng Pan, *Agency for Science, Technology and Research*, Singapore; Jörg Radnik and Jörg Manfred Stockmann, *Bundesanstalt für Materialforschung und-prüfung*, Germany; Paul Dietrich and Andreas Thissen, *SPECS Surface Nano Analysis GmbH*, Germany; Jonathan Counsell, *Kratos Analytical Ltd*, UK; Arthur Baddorf, *Oak Ridge National Laboratory*, USA; Takaharu Nagatomi, *Asahi Kasei Corporation*, Japan; Emmanuel Nolot, *Commissariat à l'énergie atomique et aux énergies alternatives (CEA-Leti)*, France; Wayne Lake, *Atomic Weapons Establishment*, UK; David Morgan, *Cardiff University*, UK; Anne Fuchs, *Robert Bosch GmbH*, Germany; Bernd Bock, *Tascon GmbH*, Germany; Jeffery Fenton, *Medtronic*, USA; David Cant, *National Physical Laboratory*, UK; Bin Cheng, *Beijing University of Chemical Technology*, China; Akira Kurokawa, Yasushi Azuma, and Lulu Zhang, *National Metrology Institute of Japan, National Institute of Advanced Industrial Science and Technology*, Japan; Andrzej Bernasik, Mateusz Marzec, and Mariusz Hajdyła, *AGH University of Science and Technology Krakow*, Poland.

APPENDIX:

1. Trigonometric relationships

Projection of the unit vector in the direction of electron emission onto the photon momentum vector from Figs. 1(a) and 1(b) provides the equalities in Eq. (A1),

$$-\cos a = \sin\theta_B \cos\phi_B = \sin\theta_A \cos\phi_A. \tag{A1}$$

If the direction of ϵ_A is parallel to $b = 0$ and $a = 90°$, then the following relationships can be found:

$$\cos\theta_A = \sin a \cos b, \tag{A2}$$

$$\cos\theta_B = \sin a \sin b, \tag{A3}$$

$$\sin^2 a = \cos^2\theta_A + \cos^2\theta_B, \tag{A4}$$

$$\sin^2 a \cos 2b = \cos^2\theta_A - \cos^2\theta_B. \tag{A5}$$

2. Expression of *G* in terms of instrumental geometry

From Eqs. (3) and (2) plus the analogous expression for x-rays with ϵ_B polarization and various trigonometric identities,

$$\begin{aligned}
G =& P_A\left(\frac{\beta}{2}(3\cos^2\theta_A - 1) + (\delta + \gamma\cos^2\theta_A)\sin\theta_A\cos\phi_A\right) + (1 - P_A)\left(\frac{\beta}{2}(3\cos^2\theta_B - 1) + (\delta + \gamma\cos^2\theta_B)\sin\theta_B\cos\phi_B\right)\\
=& -\frac{\beta}{2} - \delta\cos a + P_A\left(\frac{3\beta}{2} - \gamma\cos a\right)\cos^2\theta_A + (1 - P_A)\left(\frac{3\beta}{2} - \gamma\cos a\right)\cos^2\theta_B\\
=& -\frac{\beta}{2} - \delta\cos a + \left(\frac{3\beta}{2} - \gamma\cos a\right)[P_A(\cos^2\theta_A - \cos^2\theta_B) + \cos^2\theta_B]\\
=& -\frac{\beta}{2} - \delta\cos a + \left(\frac{3\beta}{2} - \gamma\cos a\right)[P_A\sin^2 a\cos 2b + \sin^2 a\sin^2 b]\\
=& -\frac{\beta}{2} - \delta\cos a + \left(\frac{3\beta}{2} - \gamma\cos a\right)\left[P_A\cos 2b + \frac{1}{2} - \frac{1}{2}\cos 2b\right]\sin^2 a\\
=& -\frac{\beta}{2} - \delta\cos a + \left(\frac{3\beta}{2} - \gamma\cos a\right)\left[\frac{1}{2} + \left(P_A - \frac{1}{2}\right)\cos 2b\right]\sin^2 a.
\end{aligned} \tag{A6}$$

The final form is the same as Eq. (4), we note that with $P_A = 0.5$, the equation can be simplified to the standard unpolarized expression given in Eq. (A7),

$$G(\text{unpol}) = -\frac{\beta}{4}(3\cos^2 a - 1) - \left(\delta + \frac{\gamma}{2}\sin^2 a\right)\cos a. \tag{A7}$$

3. Orthogonal angles

The angles, a', b' orthogonal to the emission direction a, b lie on the plane normal to the sample–analyzer vector. The azimuthal angle of emission from the atom within the plane is c, which has the range from 0 to 2π. Defining the unit vectors from the atom to the analyzer as [0, 0, 1], the plane of emission as $C = [\cos c, \sin c, 0]$ and the direction from the atom to the monochromator as

$D = [\sin a, 0, \cos a]$, the dot product $C{\cdot}D = |C||D|\cos a'$ of the latter two vectors provides a' as expressed in Eq. (A8). To find b', the circle defined by $[\cos c, \sin c, 0]$ is projected onto the plane which is normal to D, this projection is an ellipse described by the set of vectors $E = [-\cos a \ \cos c, \ \sin c]$, where the normalized projected vector to the analyzer is [1, 0]. Note that the set of vectors E is not normalized and have magnitude $|E| = \sqrt{E{\cdot}E}$. The angle between these projected vectors is found from their dot product and is the dihedral angle between the electron and the analyzer. This angle is the difference between b', the dihedral angle between the anode and the electron and b, the dihedral angle between the anode and the analyzer as shown in Eq. (A9),

$$\cos a' = \sin a \cos c, \tag{A8}$$

$$\cos(b' - b) = \frac{-\cos a \cos c}{\sqrt{\sin^2 c + \cos^2 a \cos^2 c}}. \tag{A9}$$

4. Angular dispersion

There are two sources of angular variation, the angular dispersion of x-rays from the monochromator and the range of analyzer collection angles. Typically, the former is <10° and the latter ranges between 5° and 30° or even more. To evaluate the importance of these effects, it is appropriate to calculate the integral of Eq. (6) with respect to angles a and b. It is easiest to write Eq. (4) in the form of Eqs. (A10)–(A14),

$$G = k_0 + \sum_{i=1}^{3} k_i \cos ia, \tag{A10}$$

$$k_0 = \frac{3\beta}{4}\left[\frac{1}{2} + \left(P_A - \frac{1}{2}\right)\cos 2b\right] - \frac{\beta}{2}, \tag{A11}$$

$$k_1 = -\delta - \frac{\gamma}{4}\left[\frac{1}{2} + \left(P_A - \frac{1}{2}\right)\cos 2b\right], \tag{A12}$$

$$k_2 = -\frac{3\beta}{4}\left[\frac{1}{2} + \left(P_A - \frac{1}{2}\right)\cos 2b\right], \tag{A13}$$

$$k_3 = \frac{\gamma}{4}\left[\frac{1}{2} + \left(P_A - \frac{1}{2}\right)\cos 2b\right]. \tag{A14}$$

Then, integration of Eq. (A10) over an angular range Δa with mean angle a_0 and normalization by the angular range yields Eq. (A15),

$$\frac{1}{\Delta a}\int_{a_0-\frac{\Delta a}{2}}^{a_0+\frac{\Delta a}{2}} G = k_0 + \sum_{i=1}^{3} k_i \cos ia_0 \frac{2\sin\left(\frac{i\Delta a}{2}\right)}{i\Delta a}, \tag{A15}$$

from which the deviation of the signal from an infinitesimal angular range can be found. This deviation is clearly a function of s and is maximal when $s = 1$. With the values for Al Kα radiation and C 1s photoemission inserted, it transpires that the value of b is of negligible importance; in fact, it is also easy to show that angular integration across a range of Δb produces little change in the normalized photoemission intensity. The important parameter is the value of a_0, at $a_0 = 40°$ there is virtually no effect of angular integration on the signal. For geometries with $a_0 > 40°$, there will be a modest change in signal, increasing with larger integration angles which, for $a_0 > 60°$, may reach 2% if $s = 1$ and $\Delta a = 30°$. More typically, the change is 1% or less. These effects are rather small in the context of this work, and, therefore, we have not taken electron collection angles or x-ray angular ranges into account.

DATA AVAILABILITY

The data that support the findings of this study are available from the corresponding author upon reasonable request.

REFERENCES

[1]D. R. Baer *et al.*, J. Vac. Sci. Technol. A **37**, 031401 (2019).
[2]M. P. Seah, J. Electron Spectr. Rel. Phenom. **71**, 191 (1995).
[3]M. P. Seah, Surf. Interface Anal. **20**, 243 (1993).
[4]M. P. Seah and G. C. Smith, Surf. Interface Anal. **15**, 751 (1990).
[5]M. P. Seah and S. J. Spencer, J. Electron Spectr. Rel. Phenom. **151**, 178 (2006).
[6]P. J. Cumpson, S. J. Spencer, and M. P. Seah, Spectrosc. Eur. **10**, 8 (1998).
[7]B. P. Reed, D. J. H. Cant, S. J. Spencer, A. J. Carmona-Carmona, A. Bushell, A. Herrera-Gómez, A. Kurokawa, A. Thissen, A. G. Thomas, A. J. Britton, A. Bernasik, A. Fuchs, A. P. Baddorf, B. Bock, B. Theilacker, B. Cheng, D. G. Castner, D. J. Morgan, D. Valley, E. A. Willneff, E. F. Smith, E. Nolot, F. Xie, G. Zorn, G. C. Smith, H. Yasufuku, J. Fenton, J. Chen, J. D. P. Counsell, J. Radnik, K. J. Gaskell, K. Artyushkova, L. Yang, L. Zhang, M. Eguchi, M. Walker, M. Hajdy, M. M. Marzec, M. R. Linford, N. Kubota, O. Cortazar-Martínez, P. Dietrich, R. Satoh, S. L. M. Schroeder, T. G. Avval, T. Nagatomi, V. Fernandez, W. Lake, Y. Azuma, Y. Yoshikawa, and A. G. Shard, J. Vac. Sci. Technol. A **38**, 063208 (2020).
[8]M. P. Seah, Surf. Interface Anal. **20**, 865 (1993).
[9]A. G. Shard and S. J. Spencer, Surf. Interface Anal. **51**, 618 (2019).
[10]A. Jablonski and C. J. Powell, Surf. Sci. **604**, 327 (2010).
[11]A. Jablonski, J. Phys. D Appl. Phys. **48**, 075301 (2015).
[12]V. Nefedov and I. Nefedova, J. Electron Spectr. Rel. Phenom. **107**, 131 (2000).
[13]M. Trzhaskovskaya and V. Yarzhemsky, Atom. Data Nucl. Data Tables **119**, 99 (2018).
[14]A. Herrera-Gomez, J. Electron Spectr. Rel. Phenom. **182**, 81 (2010).